The Effect of Polymer Optoelectronic Properties on the Performance of Multilayer Hybrid Polymer/TiO_2 Solar Cells**

By *Punniamoorthy Ravirajan*, *Saif A. Haque*, *James R. Durrant*, *Donal D. C. Bradley*, and *Jenny Nelson**

We report a study of the effects of polymer optoelectronic properties on the performance of photovoltaic devices consisting of nanocrystalline TiO_2 and a conjugated polymer. Three different poly(2-methoxy-5-(2′-ethylhexoxy)-1,4-phenylenevinylene) (MEH-PPV)-based polymers and a fluorene–bithiophene copolymer are compared. We use photoluminescence quenching, time-of-flight mobility measurements, and optical spectroscopy to characterize the exciton-transport, charge-transport, and light-harvesting properties, respectively, of the polymers, and correlate these material properties with photovoltaic-device performance. We find that photocurrent is primarily limited by the photogeneration rate and by the quality of the interfaces, rather than by hole transport in the polymer. We have also studied the photovoltaic performance of these TiO_2/polymer devices as a function of the fabrication route and device design. Including a dip-coating step before spin-coating the polymer leads to excellent polymer penetration into highly structured TiO_2 networks, as was confirmed through transient optical measurements of the photoinduced charge-transfer yield and recombination kinetics. Device performance is further improved for all material combinations studied, by introducing a layer of poly(ethylene dioxythiophene) (PEDOT) doped with poly(styrene sulfonic acid) (PSS) under the top contact. Optimized devices incorporating the additional dip-coated and PEDOT:PSS layers produced a short-circuit current density of about 1 mA cm^{-2}, a fill factor of 0.50, and an open-circuit voltage of 0.86 V under simulated AM 1.5 illumination (100 mW cm^{-2}, 1 sun). The corresponding power conversion efficiency under 1 sun was ≥ 0.4 %.

1. Introduction

Organic photovoltaic materials are under intensive study for potential application in low-cost, large-area solar cells. Power conversion efficiencies exceeding 3 % have been reported in several device configurations.[1] Although all-organic systems such as polymer/fullerene blends are receiving high interest, these systems suffer from poor photostability of the two organic components and poor mechanical stability of the active layers through phase segregation. One promising alternative approach is to use a nanostructured *inorganic* semiconductor as the electron-transport component.[2] Electron-transporting metal oxides, such as titanium dioxide (TiO_2), tin oxide (SnO_2), and zinc oxide (ZnO), are attractive materials in this context on account of their low cost, good stability, ease of fabrication, and the potential that exists for controlling their film morphology on the nanoscale.[3] Effective charge separation in metal-oxide/conjugated-polymer composites has been demonstrated and such hybrid materials are attracting growing interest for use in photovoltaics.[4–8]

The TiO_2/polymer combination is the best-studied system[4–14] for hybrid metal-oxide/polymer photovoltaic devices compared to other metal-oxide/polymer systems. However, the highest measured power conversion efficiency value reported for a TiO_2/polymer system to date is 0.18 % under 1 sun (100 mW cm^{-2}),[4] and highest external quantum efficiency (25 % at 435 nm[8]) is substantially lower than the highest efficiency for conjugated-polymer/fullerene solar cells.

Efficient photocurrent generation in polymer/TiO_2 structures requires that the TiO_2 be structured on the scale of the exciton diffusion length of the polymer (~ 5–20 nm). Originally, it was believed that incomplete polymer infiltration into highly structured or porous TiO_2 (pore size ~ 10–20 nm) would limit the performance of hybrid polymer/TiO_2 solar cells. This is no longer considered a limitation since several recent studies have shown that intimate polymer/metal-oxide infiltration can be achieved by various approaches. These include heat,[14] dip-coating of mesoporous TiO_2 films,[13,15] spin-casting on ultrathin dip-coated TiO_2 films,[6] in-situ growth of TiO_2 from an organic precursor,[11] and heat treatment of a spin-cast polymer into templated nanostructured TiO_2 substrates.[9] It should be noted that infiltration is a function of the polymer used, and that regioregular poly(3-hexyl thiophene) (RR P3HT) has been found to resist infiltration into mesoporous titania through the coiling of the polymer chains.[9] Although attempts

[*] Dr. J. Nelson, Dr. P. Ravirajan,[+] Prof. D. D. C. Bradley
Department of Physics, Imperial College London
Prince Consort Road, London SW7 2BW (UK)
E-mail: jenny.nelson@imperial.ac.uk
Dr. S. A. Haque, Dr. J. R. Durrant
Department of Chemistry, Imperial College London
Exhibition Road, London SW7 2AZ (UK)
[+] Also at the Department of Physics, University of Jaffna, Jaffna, Sri Lanka.

[**] We are grateful to Prof. H. H. Horhold for providing the MEH-PPV-based polymer samples and to Mr. Alex Green, Dr. Emillio Palomares, and Ms. Yeni Astuti for helping us to prepare TiO_2 paste and for technical assistance with cyclic voltammetry measurements. PR acknowledges the Association of Commonwealth Universities for a Commonwealth Scholarship. JN and JRD acknowledge the EPSRC for financial support. DDCB thanks The Dow Chemical Company for providing the F8T2 polymer.

DOI: 10.1002/adfm.200400165

to blend TiO_2 nanoparticles with conjugated polymers in solution have not led to efficient devices,[12,16] this route has recently been successfully exploited[17] for zinc oxide nanoparticles (~5 nm) with poly[2-methoxy-5-(3′,7′-dimethyloctyloxy)-1,4-phenylene vinylene] (MDMO-PPV) polymer. Janssen and co-workers reported[17] an efficient ITO/PEDOT:PSS/MDMO-PPV:ZnO/Al device (ITO: indium tin oxide; PEDOT: poly(ethylene dioxythiophene); PSS: poly(styrene sulfonic acid)), which showed external quantum efficiency of 40 % at the absorption maximum of the polymer.

Despite successful infiltration of polymer into thin (≤100 nm) nanostructured TiO_2 films, the power conversion efficiency is a factor of ten smaller than the best power conversion efficiency achieved using similar polymers with fullerenes. The difference is largely in the value of the short-circuit current density, J_{SC}, whilst the values of open-circuit voltage, V_{OC}, and fill factor, *FF*, are similar to the best published data for organic solar cells. The reduced J_{SC} may be due to a number of factors: limited red absorbance, small optical depth, poor sensitization of the oxide film, large pore size/nanostructure scale compared to the exciton diffusion length, poor charge transport, fast recombination, or imperfect interfaces. However, it is difficult to analyze these losses on the basis of previous studies, on account of wide variations in materials and fabrication techniques.

In this paper, we attempt to identify the mechanisms limiting the short-circuit current density, through a systematic study of the effect of the optoelectronic properties of the polymer on the performance of a model polymer/TiO_2 hybrid system. We focus on a series of poly(2-methoxy-5-(2′-ethylhexoxy)-1,4-phenylenevinylene) (MEH-PPV)-based polymers, characterized by long exciton diffusion length, and high hole mobility, and/or good red absorbance. Through complementary studies of device performance and the charge-transport and light-harvesting properties of these materials, we show that photocurrent is limited primarily by the photogeneration rate and by the quality of the interfaces, rather than by hole transport in the polymer. The corresponding devices show power conversion efficiencies of up to 0.41 % under 1 sun, approximately double the best previously reported value for a TiO_2/polymer hybrid device under the same conditions.

Four hole-conducting polymers have been used in this work and their names and structures[18–20] are shown in Figures 1a–d. The first three of these polymers have MEH-PPV subunits and the first two contain *N*,*N*′-diphenyl-*N*,*N*′-bis(3-methylphenyl)-(1,1′-biphenyl)-4,4′-diamine (TPD) groups. The TPD (4M)-MEH-M3EH-PPV polymer is a regular terpolymer while the others are alternating copolymers. The MEH-DOO-PPV copolymer has broad optical absorption in the visible spectrum peaking at about 502 nm, while the TPD-containing polymers absorb less strongly in the visible but have better hole-transport properties (see Sect. 2 below). For some studies we used a fourth polymer, a fluorene–bithiophene alternating copolymer (poly[(9,9-dioctylfluorene)-*co*-bithiophene], F8T2), which we have studied previously,[13] as a control. Figure 1e shows the optimized multilayer device structure. All devices were prepared on ITO-coated glass substrates (~1 cm^2). There are four layers: a dense TiO_2 layer, a porous TiO_2 layer, and dip-coated and spin-coated polymer layers. The dense layer prevents direct contact between the polymer and the substrate and is thus called the 'hole-blocking layer' (HBL). In some cases, a layer of PEDOT:PSS was deposited on top of the hole-transporting polymer layer before depositing the metal contact. Six devices were fabricated per substrate to check reproducibility. The full preparation details for the multilayer devices can be found in the Experimental section.

2. Results and Discussion

2.1. Polymer Hole Mobilities

The polymer hole mobilities were studied using the time-of-flight (TOF) method. Figure 2a shows a typical room-temperature hole-current transient for the TPD(4M)-MEH-PPV polymer, in an ITO/polymer (1.2 μm)/Al device structure, at 1.3×10^5 V cm^{-1}. The inset shows the corresponding transient on a double logarithmic scale. The transient shows an initial spike followed by a distinctive plateau and then by a broad tail. The constant-current plateau in the hole transient of TPD(4M)-MEH-PPV polymer indicates non-dispersive transport. The transit time, t_T, corresponding to the intercept of the asymptotes to the hole transient on a log–log scale, is about 0.9 μs and the corresponding mobility is 1×10^{-3} cm^2 V^{-1} s^{-1} at 1.3×10^5 V cm^{-1}. Hole transients for the other two polymers (data not shown) show dispersive transients but a clear transient time can be determined. The drift mobility at an applied electric field, *E*, is calculated from the expression $\mu = d/(t_T E)$, where *d* is the polymer thickness.

Figure 2b shows the electric-field-dependent variation of the room-temperature hole mobility for all three polymers. The electric field was calculated taking into account a built-in voltage of 0.3 V, namely the workfunction difference between the ITO (4.6 eV) and Al (4.3 eV) electrodes. The work-function values of ITO and Al were estimated by Kelvin-probe and electroabsorption measurements.[13] The hole mobilities of all polymers follow a Poole–Frenkel dependence $\mu_h \propto \exp(\beta E^{1/2})$.[21] The two TPD-containing polymers show higher hole mobility than the MEH-DOO-PPV polymer. This may be due to the positive influence of the TPD group on hole transport.[22] The TPD(4M)-MEH-PPV polymer shows higher hole mobility than the other two polymers in the range of electric fields from 0.9×10^5 V cm^{-1} to 5×10^5 V cm^{-1}. The TPD(4M)-MEH-PPV polymer also shows weaker field dependence, while both TPD(4M)-MEH-M3EH-PPV and MEH-DOO-PPV polymers show strong field dependence. Estimating an electric field of 1×10^5 V cm^{-1} within an efficient TiO_2/polymer photovoltaic device (polymer thickness ~50–100 nm) at short circuit, the TPD(4M) MEH-PPV polymer would be expected to give the best hole transport in devices. However, hole transport in both TPD(4M) MEH-M3EH-PPV and MEH-DOO-PPV polymers should improve in thinner devices.

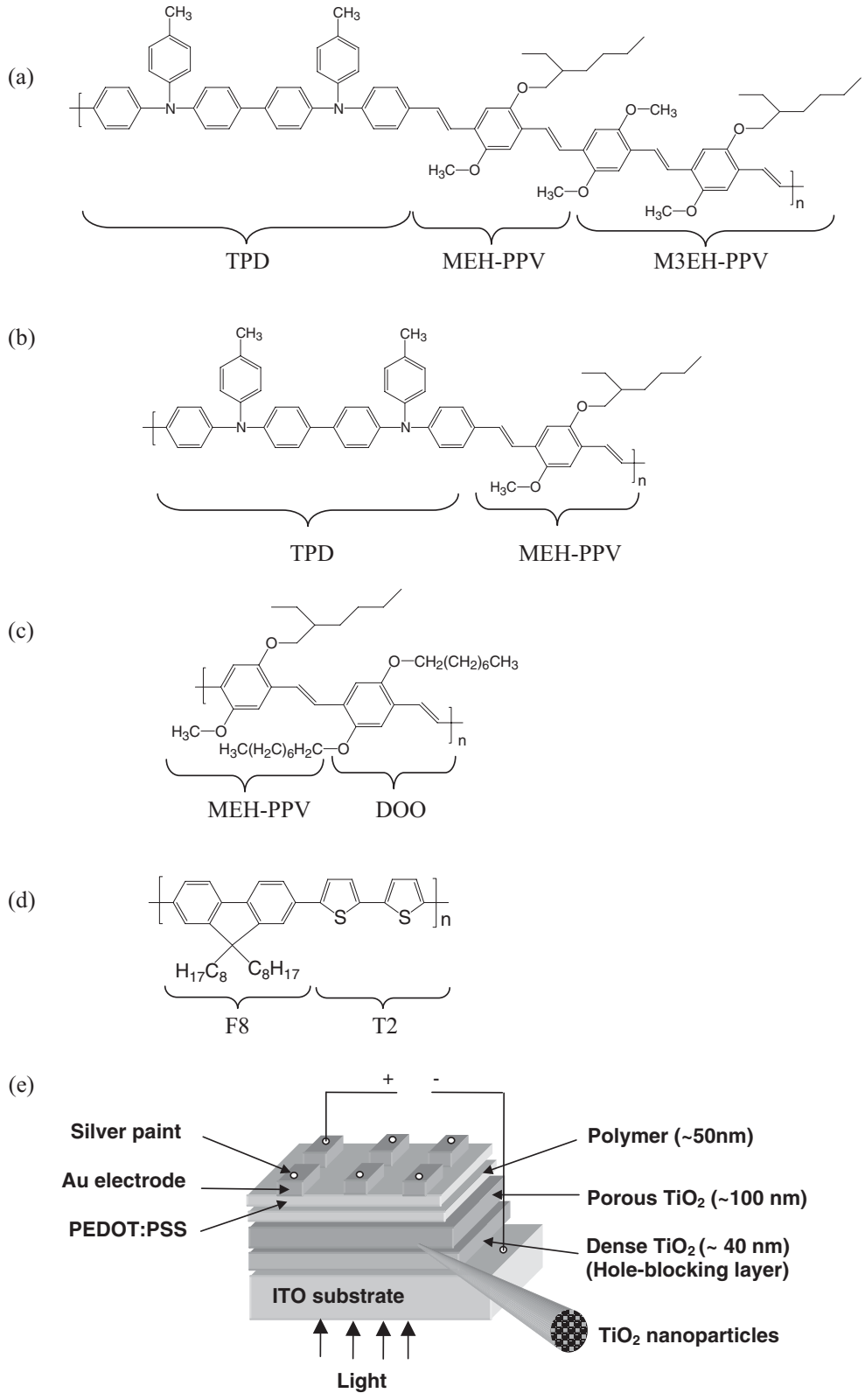

Figure 1. Chemical structures [18–20] of a) poly[(1,4-phenylene-(4-methylphenyl)amino-4,4′-diphenylene-(4-methylphenyl)amino-1,4-phenylene-ethenylene-2-methoxy-5-(2-ethylexyloxy)-1,4-phenylene-ethenylene)-*co*-(2,5-dimethoxy-1,4-phenylene-ethenylene-2-methoxy-5-(2-ethylhexyloxy)-1,4-phenylene-ethenylene)], TPD(4M)-MEH-M3EH-PPV terpolymer, b) poly[(4-methylphenyl)amino-4,4′-diphenylene-(4-methylphenyl)amino-1,4-phenylene-ethenylene-2-methoxy-5-(2-ethylhexyloxy)-1,4-phenylene-ethenylene-1,4-phenylene], TPD(4M)-MEH-PPV copolymer, c) poly[2-methoxy-5-(2-ethylhexyloxy)-1,4-phenylene-ethenylene-2,5-dioctyloxy-1,4-phenylene-ethenylene], MEH-DOO-PPV copolymer, and d) poly[(9,9-dioctylfluorene)-*co*-bithiophene], (F8T2) copolymer. e) Optimized device structure.

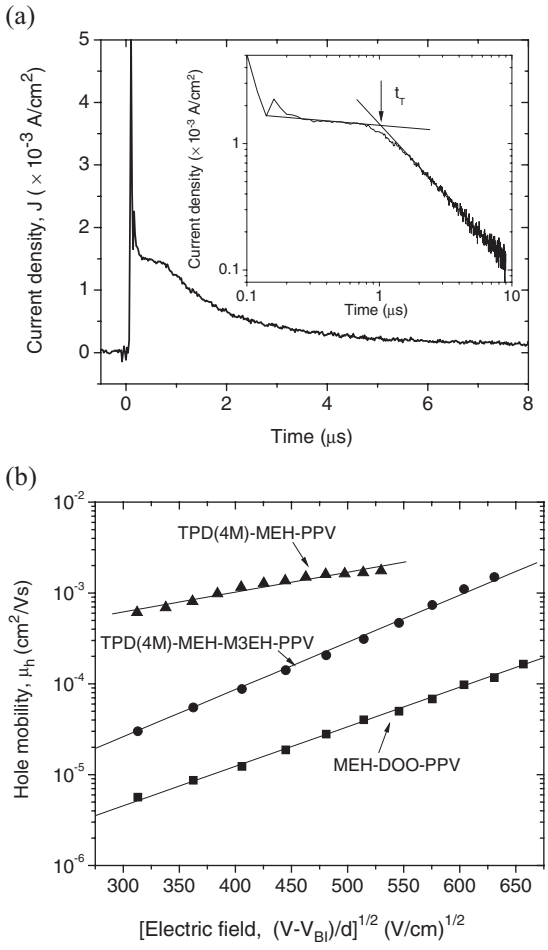

Figure 2. a) A typical room-temperature TOF hole transient in ITO/TPD(4M)-MEH-PPV (1.2 μm)/Al at an electric field 1.3×10^5 V cm^{-1}. b) Variation of the room-temperature TOF hole mobility μ_h with electric field for the three MEH-PPV-based polymers. The film thicknesses were 1.2, 1.5, and 1.5 μm for polymers TPD(4M)-MEH-PPV (triangles), TPD(4M)-MEH-M3EH-PPV (circles), and MEH-DOO-PPV (squares), respectively. The built-in voltage for the ITO/polymer/Al structure is assumed to be 0.3 V.

2.2. Polymer Absorption and Sensitization of TiO_2

Optical absorption spectra for thin films of each of the three MEH-PPV-based polymers spin-coated on spectrosil B substrates are shown in Figure 3a. The magnitude of the absorption coefficient is similar for all three polymers, but the MEH-DOO-PPV polymer absorbs further into the red, with peak absorption at 502 nm. The absorption spectrum of the TPD(4M)-MEH-M3EH-PPV polymer is red-shifted slightly compared to that of TPD(4M)-MEH-PPV. Whilst TPD(4M)-MEH-PPV and MEH-DOO-PPV are strictly alternating copolymers,[18,20] the TPD(4M)-MEH-M3EH-PPV polymer is a statistical condensation copolymer consisting of TPD(4M)-MEH-PPV $(AB)_x$ repeat units and M3EH-PPV $(CB)_y$ repeat units in the ratio $x/y = 50{:}50$.[20] The M3EH-PPV units are therefore believed to be responsible for the red shoulder in the absorption of TPD(4M)-MEH-M3EH-PPV.

Table 1 compares the ionization potential, hole transport, and absorption properties of these three PPV polymers as well as those of the fluorene–bithiophene copolymer, F8T2. The F8T2 polymer has a higher optical absorption in the visible spectrum than the two TPD polymers, peaking at about 460 nm.[13] This polymer shows highly dispersive hole transport and strongly field-dependent TOF hole mobility in the range of 10^{-5}–10^{-4} cm^2 V^{-1} s^{-1} over the electric-field range 1×10^4–6×10^4 V cm^{-1}.[23] It performs rather better as an aligned thin film in field-effect transistor structures.[24] The ionization potential of each polymer was estimated using cyclic voltammetry of the polymer film, and lies between 5.2 eV and 5.5 eV, as shown in the third column of Table 1. The last two columns of Table 1 compare the hole mobility at a given electric field and the nature of hole transport. Overall, the TPD(4M)-MEH-M3EH-PPV polymer shows the most promising combination of hole transport and absorption properties for solar-cell application.

Good uptake of polymer by the porous TiO_2 is essential for efficient device performance. Figure 3b compares the optical density of porous TiO_2 electrodes of thickness about 100 nm fol-

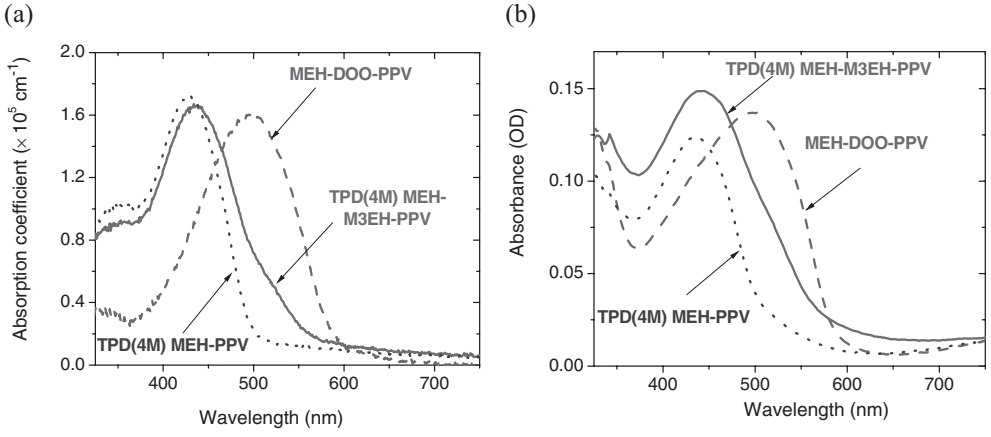

Figure 3. a) Absorption spectra of the three MEH-PPV polymers: TPD(4M) MEH-M3EH-PPV (solid line), MEH-DOO-PPV (dashed line), and TPD(4M) MEH-PPV (dotted line), deduced from UV-vis optical absorption spectra of thin polymer films on spectrosil B substrates. b) UV-vis optical absorption spectra of TiO_2 nanoporous films of thickness 100 nm, after dipping in the respective polymer/C_6H_5Cl (2 mg mL^{-1}) solutions for 18 h at 60 °C.

Table 1. Summary of optoelectronic parameters for the polymers studied. λ_{max} is the wavelength corresponding to maximum absorption, α the corresponding absorption coefficient, I_P the ionization potential, and μ_h the hole mobility at 2.5×10^5 V cm^{-1}.

Polymer	α [$\times 10^{-5}$ cm^{-1}]	λ_{max} [nm]	I_P [eV]	μ_h at 2.5×10^5 V cm^{-1} [cm^2 V cm^{-1}]	Type of transport
MEH-DOO-PPV	1.60	502	5.25	3.3×10^{-5}	Dispersive
TPD(4M)-MEH-M3EH-PPV	1.67	439	5.30	2.8×10^{-4}	Dispersive
TPD(4M)-MEH-PPV	1.74	428	5.45	2.0×10^{-3}	Non-dispersive
F8T2	2.90	460	5.55	10^{-4}	Highly dispersive

lowing dip-coating in solutions of each of the MEH-PPV-based polymers. All three sensitize the TiO_2 well. This may be due to an interaction between the TiO_2 surface and the oxygen atoms of the alkoxy substituents on the MEH-PPV subunits of each polymer.[25] The TPD(4M)-MEH-M3EH-PPV polymer shows a better uptake by TiO_2 than the other two polymers. This may be due to the higher number of alkoxy substituents in the polymer repeat unit. Another reason for the better sensitization of TPD(4M)-MEH-M3EH-PPV compared to TPD(4M)-MEH-PPV may be the lower average molar mass of the TPD(4M)-MEH-M3EH-PPV polymer than of TPD(4M)-MEH-PPV (35700 g mol^{-1} {29 repeated units} < 53 100 g mol^{-1} {66 repeated units}).[20] It was observed that polymer uptake by porous TiO_2 increases with dipping time and temperature.

2.3. Infiltration of Polymer into Porous TiO_2

Infiltration of the polymer into the porous TiO_2 film can be achieved either by heat or dip-treatment.[9,13,14] Here we show that pore filling in porous nanocrystalline TiO_2 electrodes may be improved by dip-coating. Nanosecond–microsecond spectroscopy is a useful technique for monitoring both the charge-separation yield and the charge-recombination rate in molecular photovoltaic devices.[13,14,26–28] This technique can be applied to estimate the extent of polymer penetration into porous TiO_2 in a TiO_2/polymer structure.[13,14] Comparison of the magnitude of the photoinduced absorption signal for illumination from the polymer side and from the substrate side indicates the extent of polymer penetration into the porous TiO_2. Provided that the pore volume exceeds the volume of polymer applied, complete polymer penetration results in identical photoinduced absorption signals for illumination from either side, while incomplete penetration leads to a smaller signal for illumination from the polymer side, due to the optical filtering of the pump light by the layer of polymer not incorporated into the porous film.

Figure 4 shows the transient absorption kinetics for porous TiO_2/TPD(4M)-MEH-M3EH-PPV at a probe wavelength of 750 nm and porous TiO_2/MEH-DOO-PPV at a probe wavelength of 900 nm under excitation by pulses of intensity ~ 30 μJ pulse^{-1} cm^{-2}. In each case, the probe wavelength was chosen as the maximum of the photoinduced absorption spectrum recorded after 10 μs. No photoinduced absorption signal was observed at the probe wavelength for pristine films of either polymer, therefore the observed signal for the composite films on the (0.1 μs–100 ms) timescale can safely be assigned to hole-polarons rather than to triplet states. The inset shows the sample structure. Each sample was excited at the peak absorption wavelength of the polymer (450 nm for TPD(4M)-MEH-M3EH-PPV and 500 nm for MEH-DOO-PPV).

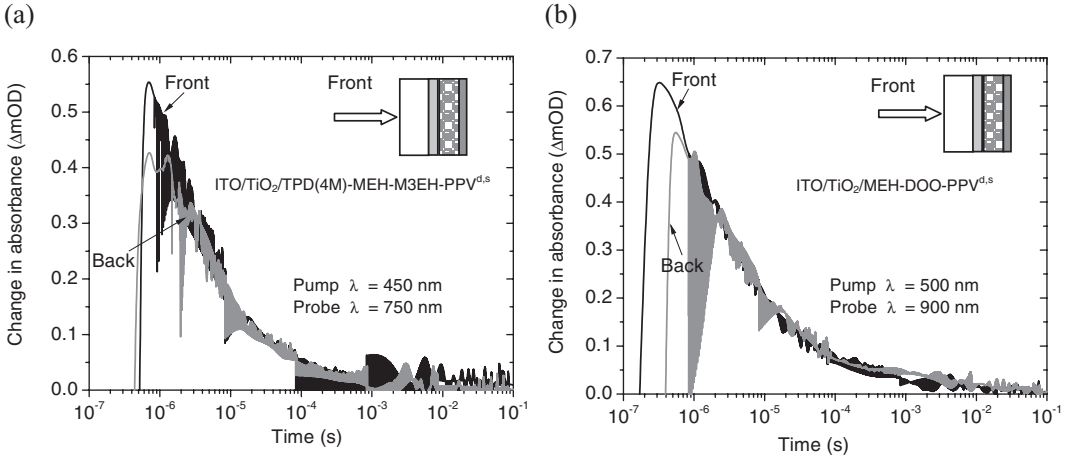

Figure 4. Transient absorption kinetics following photoexcitation of ITO/HBL/porous TiO_2/polymer using a) TiO_2/TPD(4M)-MEH-M3EH-PPV polymer and b) MEH-DOO-PPV polymer. The inset shows the sample structure: ITO/HBL/porous TiO_2/polymer^{d,s}, where the superscripts d and s indicate both 'dip-coated' and 'spin-coated' layers, respectively. The excitation density was about 30 μJ pulse^{-1} cm^{-2} (corresponding to 1.3×10^{14} incident photons pulse^{-1} cm^{-2}). The transient absorption is assigned to hole-polarons in the polymer and the decay to interfacial recombination between electrons in the TiO_2 and hole-polarons in the polymer. Black lines indicate illumination from the substrate ('front') side and gray lines correspond to illumination from the polymer ('back') side.

The layer structures of each sample are identical with layer thicknesses of about 50 nm HBL, 100 nm porous TiO_2, and about 50 nm effective polymer thickness, including both dip-coated and spin-coated layers. We estimated the effective polymer thickness on porous TiO_2 by comparing the optical absorption of the polymer-coated TiO_2 electrode with the known absorption coefficient of the respective polymer on spectrosil. The optical density of the active layers after dip- and spin-coating is about 0.3–0.4 at the pump wavelength. The shape and magnitude of the transient absorption signals are almost identical for illumination from the back (polymer side) and front (substrate side), indicating that polymer penetration is excellent in both structures. However, the decay of the signal in each case is relatively fast, with a half time of 5–10 μs, compared to the slower recombination times of 100 μs–10 ms observed previously in TiO_2/F8T2 solar cells[13,14] and dye-sensitized solar cells.[26,27] These recombination times, however, compare reasonably well with values (1–100 μs) reported for polymer/fullerene blends, which are used as the active layer in efficient organic solar cells.[29] The slightly faster charge-recombination kinetics in TiO_2/TPD (4M)-MEH-M3EH-PPV compared to TiO_2/MEH-DOO-PPV samples may be due to the higher hole mobility in the TPD (4M)-MEH-M3EH-PPV polymer.[30]

2.4 Exciton Diffusion Length

The exciton diffusion length in TPD (4M)-MEH-M3EH-PPV polymer was estimated using the method described in the literature.[7] Figure 5 shows the relative photoluminescence of the TPD(4M)-MEH-M3EH-PPV polymer layers on ITO and dense TiO_2 substrates at 600 nm, as a function of polymer-layer thickness when the polymer was excited with 450 nm light through the ITO-coated glass substrate. The photoluminescence measurements were taken using a FlouroMax 3.0 spectrofluorimeter and the insert shows the measurement geometry. The polymer-layer thickness on the dense TiO_2 layer was estimated from the UV-vis optical absorption of the layer using the known absorption coefficient of the polymer. The luminescence varies linearly with polymer layer thickness on ITO, and approximately linearly with polymer thickness on dense TiO_2. For the dense TiO_2 substrate, the trend predicts complete quenching of luminescence at a layer thickness of about 15 nm, and we can therefore estimate the exciton diffusion length in the polymer as (15 ± 4) nm. This is longer than the exciton diffusion length in F8T2 (~5 nm)[13,31] but it is similar to that in MEH-PPV (20 nm).[7] The other two PPV polymers also contain MEH-PPV sub-units and we might expect that their exciton diffusion lengths would to be similar to those of TPD(4M)-MEH-M3EH-PPV and MEH-PPV.

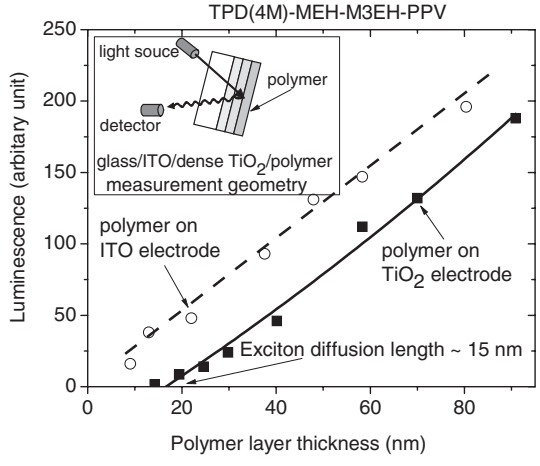

Figure 5. Photoluminescence at 600 nm from a spin-coated TPD (4M)-MEH-M3EH-PPV polymer layer on ITO (top curve) and on ITO/dense-TiO_2 (lower curve) substrates as a function of polymer-layer thickness. The polymer was excited with 400 nm light through the ITO. The inset shows the measurement geometry in the spectrofluorimeter.

2.5. Photovoltaic Device Performance

We consider now the influence of the hole-transport and light-havesting properties of the polymer on the performance of TiO_2/polymer phtovoltaic devices. Figure 6 compares the current-density–voltage (J–V) characteristics of TiO_2/polymer devices based on each of the three MEH-PPV-based polymers under AM 1.5-equivalent illumination (100 mW cm^{-2},1 sun).

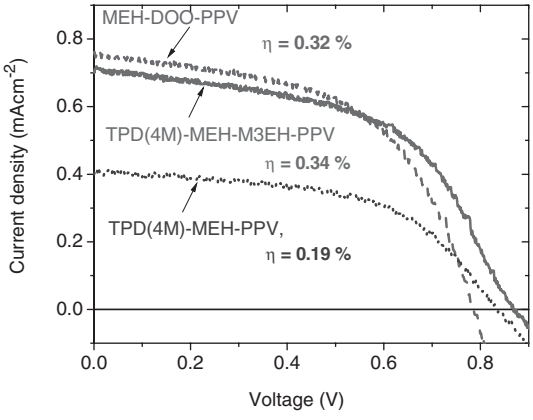

Figure 6. Current-density–voltage (J–V) characteristics of ITO/HBL (50 nm)/porous TiO_2 (100 nm)/polymer^{d,s} (50 nm)/Au devices under simulated (100 mW cm^{-2}, AM 1.5) solar illumination. The polymers used were TPD(4M)-MEH-M3EH-PPV (dashed line), MEH-DOO-PPV (solid line), and TPD-(4M)-MEH-PPV (dotted line).

The device structure and the thicknesses of the layer are as follows unless stated otherwise: ITO/HBL (50 nm)/porous TiO_2 (100 nm)/polymer (50 nm)/Au. The MEH-DOO-PPV polymer device produced the highest J_{SC}, while the TPD(4M)-MEH-M3EH-PPV polymer showed the highest V_{OC} and best overall device performance. Both MEH-DOO-PPV and TPD(4M)-MEH-M3EH-PPV polymer devices yield power conversion efficiencies more than 0.32 % under 1 sun, which is at least 50 % higher than the best previously reported efficiency for a hybrid TiO_2/polymer solar cell.[4] The device with the

highest-hole-mobility polymer, TPD(4M)-MEH-PPV, produced the lowest $J_{SC,}$ of only 0.4 mA cm^{-2}, which can be attributed to the blue-shifted absorption and relatively poor sensitization by this polymer. Nevertheless, the power conversion efficiency of this blue polymer device, at 0.19 %, exceeds the best previously reported efficiency for a TiO_2/polymer device under 1 sun.

As stated above, the J_{SC} of a TiO_2/polymer photovoltaic device may depend upon the polymer through its light-harvesting or hole-transport properties. The low J_{SC} observed for the highest-mobility TPD(4M)-MEH-PPV polymer, with mobility more than two orders of magnitude greater than for the MEH-DOO-PPV polymer, indicates that in these devices, light harvesting plays a more important role than charge transport in determining J_{SC}. The highest device efficiency is obtained for the polymer with intermediate light-harvesting and charge-transport properties, TPD(4M)-MEH-M3EH-PPV. The larger V_{OC} for TPD(4M)-MEH-M3EH-PPV than for MEH-DOO-PPV polymer devices may result from either the higher hole mobility, the larger separation between the highest occupied molecular orbital (HOMO) level of the polymer and the conduction band of TiO_2, or both. The influence of the hole mobility on overall device performance cannot, therefore, be ruled out.

As a control, bilayer devices comprising ITO/dense TiO_2 (50 nm)/polymer (50 nm)/Au were prepared for all three polymers. In each case the efficiency was around 0.04 % under 1 sun, which is at least five times smaller than that of the device containing an additional porous TiO_2 layer. This observation confirms our previous report that the device performances improve by more than a factor of five when a thin porous TiO_2 layer is introduced into a bilayer device.[14]

2.6. Optimizing Device Design

Although the J_{SC} values reported above for two of the polymers are the highest reported to date for polymer/TiO_2 devices, they are still low compared to those achievable using similar polymers in polymer/fullerene devices.[32] Since it appears that the hole mobility is not the primary limiting factor, we also addressed the effect of the hole-collecting top contact. The Au top contact in our devices may limit photocurrent collection in several ways. First, the low effective work-function of Au when evaporated on top of polymer films[33] leads to a relatively small electric field to assist charge collection at short circuit. The low Au work function may also lead to an energy step at the interface with a high-I_P (I_P: ionization potential) polymer, which, as we have shown recently,[34] may reduce the rate of hole collection. Finally, potential damage to the polymer surface from evaporated gold may enhance the probability of exciton quenching near that interface. Therefore, we have studied the effect of introducing a PEDOT:PSS layer between polymer and top Au contact on the photovoltaic performance of TiO_2/polymer devices based on all three MEH-PPV-based polymers and on F8T2.

Figure 7 shows the effect of a PEDOT:PSS layer under the Au electrode on the J–V characteristics of TiO_2/polymer multilayer devices under AM 1.5 illumination. The additional lines in Figure 7a show the effect of a PEDOT:PSS layer on the J–V characteristics of an ITO/HBL (50 nm)/MEH-DOO-PPV/Au bilayer device under the same conditions. Table 2 compares the effect of the PEDOT:PSS layer on the photovoltaic parameters of the bilayer device. Short-circuit current densities of all devices increase by at least 30 % upon introduction of PEDOT:PSS, and the overall power conversion efficiencies are significantly improved. The photovoltaic parameters of our devices are compared with the best previously reported polymer/

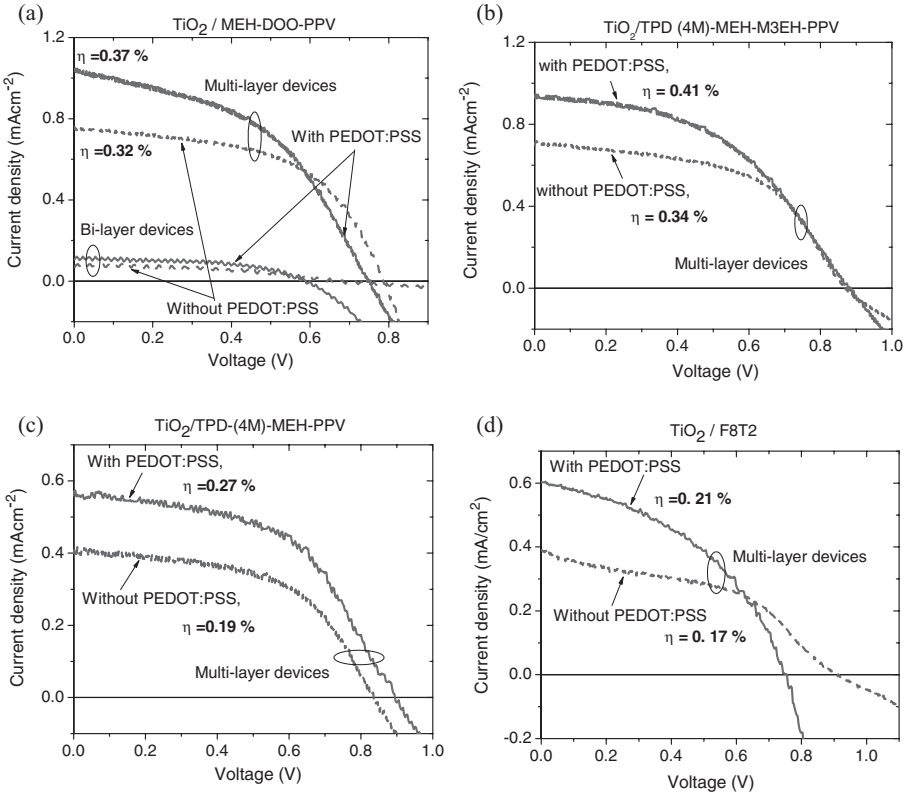

Figure 7. J–V characteristics of ITO/HBL(50 nm)/porous TiO_2 (100 nm)/polymer (50 nm)/Au devices with and without a PEDOT:PSS layer under the Au top contact. The polymers used were a) MEH-DOO-PPV, b) TPD(4M)-MEH-M3EH-PPV, c) TPD-(4M)-MEH-PPV, and d) F8T2. In each case, the solid (dashed) lines represent the J–V characteristic of the device with (without) a PEDOT:PSS layer. The additional lines in (a) show the J–V characteristic of an ITO/HBL (50 nm)/TPD(4M)-MEH-M3EH-PPV (50 nm)/Au bilayer devices with and without a PEDOT:PSS layer under the Au contact. All the measurements were performed under simulated (100 mW cm^{-2}, AM 1.5) solar illumination. J–V behavior was reproducible between different devices of the same structure, such that the standard deviation of the data is less than 10–15 %.

Table 2. The photovoltaic parameters of an ITO/HBL (50 nm)/MEH-DOO-PPV/Au bilayer device with and without a PEDOT:PSS layer the Au top contact, measured under AM 1.5 conditions (100 mW cm^{-2}, 1 sun). The values correspond to the *J–V* characteristics of the bilayer device shown in Figure 7a.

Device	J_{SC} [μA cm^{-2}]	V_{OC} [mV]	FF	η [%]
Without PEDOT:PSS	73	648	0.528	0.025
With PEDOT:PSS	123	583	0.549	0.039

TiO_2 devices in Table 3. The efficiency values for all of our devices that contain a PEDOT:PSS layer are higher than the previous best reported values.

Note that although the F8T2 polymer has comparable hole mobility and better red absorption than the TPD(4M)-MEH-M3EH-PPV polymer, F8T2-based polymer devices show a lower J_{SC}. This is probably due to the apparently shorter exciton diffusion length of the F8T2 polymer (~5 nm),[31] stressing another key factor, apart from light harvesting, in photocurrent generation.

The V_{OC} decreases upon introduction of a PEDOT:PSS layer in all devices except for the high-hole-mobility TPD(4M)-MEH-PPV polymer device, where both J_{SC} and V_{OC} increase. The more general reduction in V_{OC} can be explained in terms of the reduced interfacial energy step at the polymer–top-contact interface upon replacing Au (effective work-function 4.9 eV[13]) with PEDOT:PSS (work-function (5.2±0.1) eV). The reduced barrier for hole injection tends to increase the injected current and reduce V_{OC}, since the open-circuit voltage of a solar cell is limited by, amongst other factors,[35] currents injected from the electrodes opposing the photocurrent. Increased charge injection is also evident in the dark currents of PEDOT:PSS containing devices in all cases.

The effect of PEDOT:PSS in increasing J_{SC} may have several explanations. As noted above, these include the possible reduction in exciton quenching by the metal contact, and the effect of a larger internal electric field to assist exciton dissociation in the polymer layer. A further reason may be the improved charge transfer between polymer and top contact, resulting from the lower energy step.[34] It has already been reported that the J_{SC} and quantum efficiency of a TiO_2/polymer bilayer device increase when the energy step at the polymer–metal interface is reduced.[13] The improvement of J_{SC} may be partly due to doping of the polymer by PEDOT:PSS, and this and other possible reasons are discussed in detail in a separate publication.[36] We note that the qualitatively similar effect of PEDOT:PSS on the performance of devices using three polymers with different chemical structure shows that the mechanism responsible is quite general and is unlikely to result from an anomalous interaction between polymer and PEDOT:PSS. Instead, it seems that the roles of the PEDOT:PSS layer in improving hole injection and improving the quality of the interface are responsible.

In summary, the device with TPD(4M)-MEH-M3EH-PPV polymer, the material with the best combination of hole-transport, ionization-potential, and light-absorption properties shows the best performance. The fluorene–thiophene-copolymer device shows poorer performance than the MEH-PPV-based polymer devices, despite having similar or better light-absorption and charge-transport properties. This is probably due to a shorter exciton diffusion length for this polymer.

Although the reported efficiencies here are greater than previously published values for TiO_2/polymer solar cells, they are still lower than for polymer/fullerene solar cells, largely on account of relatively low J_{SC} values. Possible reasons may be the poor electron mobility of the porous TiO_2 (~10^{-6}-10^{-7} cm^2 V^{-1} s^{-1}[37]), the limited length scale of the nanostructure which may still allow exciton quenching despite the relatively long exciton diffusion length of MEH-PPV polymers, or the optical transparency of the TiO_2, which contributes nothing to light harvesting. Future study will therefore focus on optimizing the metal-oxide layer, in terms of its electron mobility, pore volume, and morphology.

3. Conclusion

We have studied the effects of conjugated-polymer optoelectronic properties on the performance of a model polymer/TiO_2 hybrid system. A comparison of the exciton-transport, charge-transport, and light-harvesting properties of three different MEH-PPV-based polymers and a fluorene–bithiophene polymer was made. The performance of the corresponding photovoltaic devices was also assessed. Our results established that the short-circuit current density is limited primarily by the photogeneration rate, and by the quality of the interfaces, rather than by the hole-transport properties of the polymer. Through a study of the sensitization process and device design we found that excellent polymer infiltration into the porous metal oxide could be achieved by

Table 3. The photovoltaic parameters of our multilayer TiO_2/polymer devices (shown in Fig. 7) under AM 1.5 conditions (100 mW cm^{-2}, 1 sun) are compared with the best reported devices in the literature.

Polymer	PEDOT:PSS	J_{SC} [mA cm^{-2}]	V_{OC} [V]	FF	η [%]	Reference
P3UBT	×	0.45	0.67	0.29	0.09	[10]
MEH-PPV	×	0.40	1.1	0.42	0.18	[4]
F8T2	×	0.40	0.92	0.45	0.17	[13]
	√	0.60	0.75	0.46	0.21	This work
TPD(4M)-MEH-PPV	×	0.41	0.83	0.56	0.19	This work
	√	0.57	0.90	0.53	0.27	This work
MEH-DOO-PPV	×	0.74	0.78	0.56	0.32	This work
	√	1.04	0.74	0.48	0.37	This work
TPD(4M)-MEH-M3EH-PPV	×	0.70	0.89	0.55	0.34	This work
	√	0.96	0.86	0.50	0.41	This work

dip-coating, and that including a PEDOT:PSS layer beneath the top Au contact improves the short-circuit photocurrent in all cases. An improved TiO_2/polymer device incorporating both dip-coated and PEDOT:PSS layers produced a short-circuit current density of about 1 mA cm^{-2}, a fill factor of 0.50, and an open-circuit voltage of 0.86 V under 1 sun. The corresponding overall power conversion efficiencies of these devices were ≥ 0.4 % under 1 sun.

4. Experimental

All devices were prepared on ITO-coated glass substrates (~ 1 cm^2), which were first cleaned by ultrasonic agitation in acetone and isopropanol. Two types of device structure were prepared: bilayer and multilayer. In bilayer device structures, there are two active layers, a dense TiO_2 layer and a polymer layer, while in multilayer devices there are additional active layers such as porous TiO_2 and dip-and spin-coated polymer semiconductor layers. In some devices, a PEDOT:PSS layer was also introduced between the polymer semiconductor and metal contact (Au). The ITO substrate was first covered with a thin, dense TiO_2 layer using a spray-pyrolysis technique [38]. The porous TiO_2 layer of thickness about 100 nm was deposited by spin-coating (2000 rpm (rpm: revolutions per minute)) diluted aqueous colloidal TiO_2 paste on to the dense TiO_2 layer. The layers were then sintered at 450 °C for 30 min in air. The dip-coated layer was prepared on the porous TiO_2 layer by immersing the TiO_2 electrode in a solution of polymer in C_6H_5Cl (~ 2 mg mL^{-1}) at 40–60 <M0>C for periods ranging from 6–18 h. The dip-coated film was then "wiped" by a quick blow with dry nitrogen gas (oxygen-free) and heated at about 50 °C in air. A 50 nm polymer layer was then deposited on the substrate by spin-coating from a polymer solution in C_6H_5Cl (10 mg mL^{-1}) at 2000 rpm. The thickness of each of the films on both ITO and spectrosil was measured by a Tencor Alpha-Step 200 profilometer, while the effective polymer thickness on porous TiO_2 was estimated by comparing the optical absorption of the polymer-coated TiO_2 electrode with the known absorption coefficient of the polymer on spectrosil, assuming that the TiO_2 is ~ 50 % porous. In some devices PEDOT:PSS layer was deposited on top of the polymer layer before depositing the metal contact. The deposition of PEDOT:PSS on top of the polymer is somewhat tricky as we normally observe less sensitization for PEDOT:PSS with polymer if we do not adopt the following procedures: The PEDOT:PSS solution was first untrasonicated for 15 min and then heated for 15 min at 90 °C. The solution was then filtered with a 0.45 μm filter and spin-coated on the dried semiconducting-polymer layer in a water-free environment. The sample was then annealed at 100 °C for 5 min under N_2 gas. It is essential that the PEDOT:PSS layer should be annealed for not more than 15 min because a longer annealing time degrades the layer [39]. Au electrodes were deposited either onto the semiconducting-polymer film or the PEDOT:PSS film by thermal evaporation though a shadow mask. There were six devices per substrate to check reproducibility and the area each active device was about 4.2 mm^2. The Au-contacted devices were annealed again at 100 °C for 5 min in a N_2-gas environment. The thicknesses of the layers was as follows unless stated otherwise: HBL(~ 40 nm)/porous TiO_2 (~ 100 nm)/polymer (~ 50 nm)/PEDOT:PSS (~ 50 nm)/Au (~ 70 nm). Samples for TOF measurements were also prepared on ITO and the top contact was aluminum (~ 100 nm). The thickness of semiconducting polymer in the TOF sample was typically between 1 and 1.5 μm. The *J–V* measurements were taken in air with a solar simulator (Sciencetech) and AM 1.5 spectral filter. Calibration of the light was achieved using a band-pass filter of known transmission combined with a silicon photodiode with independently certified spectral response. The lamp (high-pressure xenon-type) intensity was adjusted to give close (±5 %) agreement with the theoretical AM 1.5 photon flux over the spectral region of the polymer absorption as described in the literature [27]. Photoinduced charge-transfer yield and recombination kinetics were measured in samples without any top contact using nanosecond–millisecond transient optical spectroscopy as described elsewhere [13]. The relative luminescence intensity at 600 nm was measured as a function of polymer thickness spin-coated on ITO-coated substrates and with an additional 50 nm dense TiO_2 layer. A FluoroMax 3.0 spectrofluorimeter was used for this with 440 nm excitation through the substrate. Room temperature TOF measurements were made using a Nd:YAG frequency-tripled laser ($\lambda = 355$ nm, $\tau = 6$ ns, 2 Hz) as the excitation source. The sample was illuminated from the ITO side. Care was taken to keep the generated charge less than 5 % of the capacitor charge stored on the sample to avoid space–charge effects. Cyclic voltammetry measurements were also carried out to determine the ionization potential of all four polymers using a standard three-electrode cell comprising a Pt wire as counter-electrode, the polymer film on conducting glass as the working electrode, and an Ag/AgCl reference electrode. A redox inactive electrolyte (0.1 M tetrabutylammonium tetrafluoroborate) was used to minimize the effect of transport of analyte through migration to the working electrode. The electrolyte solution was prepared in a glovebox filled with dry nitrogen gas.

Received: April 19, 2004
Final version: September 22, 2004

[1] a) Y. Kim, S. A. Choulis, S. Cook, J. R. Durrant, J. Nelson, D. D. C. Bradley, *Appl. Phys. Lett.* **2005**, *86*, 063 502. b) F. Padinger, R. S. Rittberger, N. S. Sariciftci, *Adv. Funct. Mater.* **2003**, *13*, 85. c) M. M. Wienk, J. M. Kroon, W. J. H. Verhees, J. Knol, J. C. Hummelen, P. A. van Hal, R. A. J. Janssen, *Angew. Chem. Int. Edit.* **2003**, *42*, 3371. d) C. J. Brabec, S. E. Shaheen, C. Winder, N. S. Sariciftci, P. Denk, *Appl. Phys. Lett.* **2002**, *80*, 1288. e) P. Peumans, S. R. Forrest, *Appl. Phys. Lett*. **2001**, *79*, 126. f) J. Kruger, R. Plass, M. Gratzel, H. J. Matthieu, *Appl. Phys. Lett*. **2002**, *81*, 367.

[2] a) W. U. Huynh, J. J. Dittmer, A. P. Alivisatos, *Science* **2002**, *295*, 2425. b) J. Nelson, *Curr. Opin. Solid State Mater. Sci.* **2002**, *6*, 87.

[3] M. Gratzel, *Nature* **2001**, *414*, 338.

[4] A. J. Breeze, Z. Schlesinger, S. A. Carter, P. J. Brock, *Phys. Rev. B* **2001**, *64*, 125 205.

[5] K. M. Coakley, M. D. McGehee, *Appl. Phys. Lett.* **2003**, *83*, 3380.

[6] Q. Fan, B. McQuillin, D. D. C. Bradley, S. Whitelegg, A. B. Seddon, *Chem. Phys. Lett.* **2001**, *347*, 325.

[7] T. J. Savenije, J. M. Warman, A. Goossens, *Chem. Phys. Lett.* **1998**, *287*, 148.

[8] A. C. Arango, L. R. Johnson, V. N. Bliznyuk, Z. Schlesinger, S. A. Carter, H. H. Horhold, *Adv. Mater.* **2000**, *12*, 1689.

[9] K. M. Coakley, Y. X. Liu, M. D. McGehee, K. L. Frindell, G. D. Stucky, *Adv. Funct. Mater.* **2003**, *13*, 301.

[10] C. D. Grant, A. M. Schwartzberg, G. P. Smestad, J. Kowalik, L. M. Tolbert, J. Z. Zhang, *J. Electroanal. Chem.* **2002**, *522*, 40.

[11] P. A. van Hal, M. M. Wienk, J. M. Kroon, W. J. H. Verhees, L. H. Slooff, W. J. H. van Gennip, P. Jonkheijm, R. A. J. Janssen, *Adv. Mater.* **2003**, *15*, 118.

[12] A. C. Arango, S. A. Carter, P. J. Brock, *Appl. Phys. Lett.* **1999**, *74*, 1698.

[13] P. Ravirajan, S. A. Haque, J. R. Durrant, D. Poplavskyy, D. D. C. Bradley, J. Nelson, *J. Appl. Phys.* **2004**, *95*, 1473.

[14] P. Ravirajan, S. A. Haque, D. Poplavskyy, J. R. Durrant, D. D. C. Bradley, J. Nelson, *Thin Solid Films* **2004**, *451–452*, 624.

[15] a) S. A. Haque, E. Palomares, H. M. Upadhyaya, L. Otley, R. J. Potter, A. B. Holmes, J. R. Durrant, *Chem. Commun.* **2003** 3008. b) S. A. Haque, T. Park, C. Xu, S. Koops, N. Schulte, R. J. Potter, A. B. Holmes, J. R. Durrant, *Adv. Funct. Mater.* **2004**, *14*, 435.

[16] J. S. Salafsky, *Phys. Rev. B* **1999**, *59*, 10885.

[17] W. J. E. Beek, M. M. Wienk, R. A. J. Janssen, *Adv. Mater.* **2004**, *16*, 1009.

[18] H. H. Horhold, H. Tillmann, C. Bader, R. Stockmann, J. Nowotny, E. Klemm, W. Holzer, A. Penzkofer, *Synth. Met.* **2001**, *119*, 199.

[19] S. Pfeiffer, H. H. Horhold, *Synth. Met.* **1999**, *101*, 109.

[20] W. Holzer, A. Penzkofer, H. Tillmann, D. Raabe, H. H. Horhold, *Opt. Mater.* **2002**, *19*, 283.
[21] H. Bassler, *Phys. Stat. Sol. B* **1993**, *175*, 15.
[22] a) M. Stolka, J. F. Yanus, D. M. Pai, *J. Phys. Chem.* **1984**, *88*, 4707. b) H. H. Fong, K. C. Lun, S. K. So, *Chem. Phys. Lett.* **2002**, *353*, 407.
[23] R. Rawcliffe, private communication.
[24] H. Sirringhaus, R. J. Wilson, R. H. Friend, M. Inbasekaran, W. Wu, E. P. Woo, M. Grell, D. D. C. Bradley, *Appl. Phys. Lett.* **2000**, *77*, 406.
[25] S. Luzzati, M. Basso, M. Catellani, C. J. Brabec, D. Gebeyehu, N. S. Sariciftci, *Thin Solid Films* **2002**, *403*, 52.
[26] a) S. A. Haque, T. Park, A. B. Holmes, J. R. Durrant, *ChemPhysChem* **2003**, *4*, 89. b) J. Kruger, R. Plass, L. Cevey, M. Piccirelli, M. Gratzel, U. Bach, *Appl. Phys. Lett.* **2001**, *79*, 2085.
[27] E. Palomares, J. N. Clifford, S. A. Haque, T. Lutz, J. R. Durrant, *J. Am. Chem. Soc.* **2003**, *125*, 475.
[28] I. Montanari, J. Nelson, J. R. Durrant, *J. Phys. Chem. B* **2002**, *106*, 12203.
[29] I. Montanari, A. F. Nogueira, J. Nelson, J. R. Durrant, C. Winder, M. A. Loi, N. S. Sariciftci, C. Brabec, *Appl. Phys. Lett.* **2002**, *81*, 3001.
[30] S. A. Choulis, J. Nelson, Y. Kim, D. Poplavskyy, T. Kreouzis, J. R. Durrant, D. D. C. Bradley, *Appl. Phys. Lett.* **2003**, *83*, 3812.
[31] P. Ravirajan, A. Green, S. A. Haque, J. R. Durrant, D. D. C. Bradley, J. Nelson, *Proc. SPIE Int. Soc. Opt. Eng.*, in press.
[32] S. E. Shaheen, C. J. Brabec, N. S. Sariciftci, F. Padinger, T. Fromherz, J. C. Hummelen, *Appl. Phys. Lett.* **2001**, *78*, 841.
[33] A. J. Campbell, D. D. C. Bradley, T. Virgili, D. G. Lidzey, H. Antoniadis, *Appl. Phys. Lett.* **2001**, *79*, 3872.
[34] J. Nelson, J. Kirkpatrick, P. Ravirajan, *Phys. Rev. B* **2004**, *69*, 035 337.
[35] J. Nelson, *The Physics of Solar Cells*, Imperial College Press, London **2003**.
[36] P. Ravirajan, S. A. Haque, J. R. Durrant, H. J. P. Smit, J. M. Kroon, D. D. C. Bradley, J. Nelson, *Appl. Phys. Lett.* unpublished.
[37] B. O. Aduda, P. Ravirajan, K. L. Choy, J. Nelson, *Intern. J. Photoenergy* **2004**, *6*, 141.
[38] L. Kavan, B. O'Regan, A. Kay, M. Gratzel, *J. Electroanal. Chem.* **1993**, *346*, 291.
[39] J. Huang, P. F. Miller, J. C. de Mello, A. J. de Mello, D. D. C. Bradley, *Synth. Met.* **2003**, *139*, 569.

